Mathematical Model of the Process of Volumetric Induction Heating of Cylindrical Pieces

Bogdan Gilev [1], Hristo Ibrishimov [2], Nikolay Hinov [3]

[1] *Department of Stochastics and Optimization,Technical University of Sofia, 8 Kliment Ohridski blvd., 1000 Sofia, Bulgaria*
[2]*Department of Electric Power Supply and Equipment, Technical University of Gabrovo, 4 H. Dimitar str., 5300 Gabrovo, Bulgaria*
[3]*Faculty of Electronic Engineering and Technologies, Technical University of Sofia, 8 Kliment Ohridski blvd., 1000 Sofia, Bulgaria*

Abstract **– The present paper considers a mathematical model of the process of volumetric induction heating of cylindrical pieces in a cylindrical inductor. The model is based on a machine for volumetric induction heating of R–ITO–630/1–A–L type with a SMK UB 2F2 power source. The inductor equivalent parameters have been calculated. To verify the results obtained from the model, a 2D model has been built in Comsol Multiphysics.**

Keywords **– mathematic model, induction heating, electromagnetic field, temperature field.**

1. Introduction

There are technological processes which are unlikely to be implemented without induction heating [1]. That type of heating leads to high quality of heating at different process rates, pollution reduction, achievement of high temperatures, a possibility for using the process at high pressure and vacuum, a possibility for accurate energy dosage and availability of several control channels[2], [3].

DOI: 10.18421/TEM83-01
https://dx.doi.org/10.18421/TEM83-01

Corresponding author: Nikolay Hinov,
Faculty of Electronic Engineering and Technologies, Technical University of Sofia, Sofia, Bulgaria
Email: hinov@tu-sofia.bg

Received: 24 April 2019.
Revised: 11. June 2019.
Accepted: 17 June 2019.
Published: 28 August 2019.

Induction heating contributes to energy efficiency of the respective technology, low cost of the respective product in comparison with other volumetric heating methods, higher product quality and higher productivity.

Depending on the specific application of induction heating (tempering, volumetric heating, melting, etc.), pieces need to be heated to different temperatures and different depths of machining [4], [5], [6].

With volumetric induction heating of pieces, it is necessary to set the same temperature across the entire piece cross-section or minimum difference between the center and surface of up to 150 °C. The requirement of minimum temperature difference demands a selection of power source operating frequencies where the currents induced in the piece flow across the entire cross-section, and heating to be done in depth [1]. On the other hand, the decrease of the inductor electrical efficiency is considered. Actually, we operate with a specified penetration depth which is less than the piece radius. To reduce the temperature gradient across the cross-section, it is necessary to operate with less specific heating power from 0,05 to 0,2 kW/cm^2 and longer heating time (from tens of seconds to tens of minutes). With forging and pressing, steel pieces need to be heated up to temperature of 1200 – 1300 °C [1], [2]. With induction heating, inductors longer than the very piece are used thus achieving admissible power source energy parameters and time for producing uniform temperature across the piece cross-section (uniform heating across piece cross-section). Another important parameter is productivity (kg/h), which is mainly determined by two factors: the magnitude of the specific power set in the detail and the heating time. The specific power set in the detail defines the heating rate whereas the heating time makes possible the definition of the total amount of the heat energy set in the detail, which helps calculate the temperature been reached [1].

With volumetric induction heating of ferromagnetic pieces, the strengths of the magnetic field H and electric field E are pseudo-sinusoidal. Another distinguishing feature is that the electromagnetic and the thermal field depend on the change of parameters C, λ and σ, which characterize the conducting medium. However, the strongest non-linear characteristic of the medium is the magnetic permeability μ. In general, all parameters depend on temperature and magnetic flux density, respectively magnetic-field strength. With induction heating, they define the penetration depth Δ in the conducting body of the plane electromagnetic wave, which further complicates the process of finding a solution. This problem has been simplified by considering a model where heating is modeled in two phases. The first one is heating below the Curie point whereas the second one is heating at the Curie point (assumed to be 780 °C). At each phase parameters are averaged and the transition from the first values to the next ones is incremental thus leading to a sharp change of the simulated temperature field around the Curie point. Actually, there is no such a sharp change around the Curie point in the piece being heated. Nevertheless, it is shown in [2], [4], [5] that within heating which does not require very high heating rate (e.g. 1000 °C per 10 s), this inaccuracy of the simulated temperature field is of local nature, i.e. it occurs only around the Curie point.

The present paper aims at implementing an electromagnetic and temperature model of the volumetric induction heating process, which are intended to simulate the operation of a volumetric heating machine of R–ITO–630/1–A–L type (Fig. 2.).

2. Mathematical model

2.1. Electromagnetic problem

To solve the electromagnetic problem, Maxwell equations are used [7]:

$$\nabla \times E = -\frac{\partial B}{\partial t}, \nabla \times H = J + \frac{\partial D}{\partial t}, \quad (1)$$

where: J – density of induced current; E, H – vectors of, respectively, electric and magnetic field strength; B,D – vectors of magnetic and electric flux density; t – time, $\nabla = \frac{\partial}{\partial x}\vec{i} + \frac{\partial}{\partial y}\vec{j} + \frac{\partial}{\partial z}\vec{k}$ - nabla operator.

The dependencies characterizing the properties of the medium where the field propagates are used

$$B = \mu_0 \mu H \ , \ D = \varepsilon_0 \varepsilon E \ \text{and} \ J = \sigma E \ . \quad (2)$$

where σ – conductivity of the material; ε,μ - respectively, permitivity and permeability of the material; ε_0, μ_0 – respectively, electric and magnetic constant.

Of course, equations and constitute an integral part of Maxwell equations but they will not be included in the system (1).

After substituting (2) in (1), Maxwell equations take the form of:

$$\nabla \times E = -\mu\mu_0 \frac{\partial H}{\partial t}, \nabla \times H = \sigma E + \varepsilon\varepsilon_0 \frac{\partial E}{\partial t}. \quad (3)$$

The current in the inductor most often changes sinusoidally over time. Therefore, and also change sinusoidally. If the circular frequency of this sinusoidal law is ω, then the solutions of (3) can be found in the form

$$E(t) = E_m e^{j\tau} e^{j\omega t} = E e^{j\omega t} \text{ and } H(t) = H_m e^{j\psi} e^{j\omega t} = H e^{j\omega t},$$

where $E=E_m e^{j\tau}$, $H=H_m e^{j\Psi}$ and j is a complex unit ($j^2=-1$).

After substituting E and H in (3), the following is obtained

$$\nabla \times E = -j\mu\mu_0\omega H, \nabla \times H = \sigma E + j\varepsilon\varepsilon_0\omega E \ . \quad (4)$$

Despite the identical symbols, it should be taken into consideration that in equalities (4) quantities E and H are complex vectors whereas in (3) they are real vectors.

The following problem is presented – a plane parallel wave propagating in a semi-constrained flat body in the 3D half-space illustrated in Fig. 1a. Quantities E and H have only one constituent $H=(0,0,H_z)$ and $E=(0,E_y,0)$, i.e. the electric and magnetic field strengths have non-zero components only in the direction of the z and y axes. In this case, it is assumed that the direction of the x axis is towards the inside of the semi-constrained flat body.

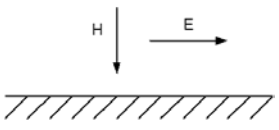

Figure 1a. Plane-parallel electromagnetic wave in a semi-constrained flat body

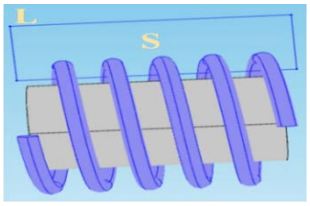

Figure 1b. Boundary condition.

System (4) takes the form:

$$\frac{d(E_y)}{dx} = -j\omega\mu\mu_0 H_z$$
$$-\frac{dH_z}{dx} = (\sigma + j\omega\varepsilon\varepsilon_0)E_y. \quad (5)$$

After differentiating the second equation and substituting the first equation in the second one, we obtain the following equation

$$\frac{d^2H_z}{dx^2} - k^2 H_z = 0, \quad (6)$$

where $k^2 = j\sigma\omega\mu\mu_0 - \omega^2\mu\mu_0\varepsilon\varepsilon_0$.

With conductive materials, the real part of κ^2 could be neglected due to its low value. Therefore, for κ the following is obtained:

$$k \approx \sqrt{j\sigma\omega\mu\mu_0} = (1+j)\sqrt{\frac{\sigma\omega\mu\mu_0}{2}} = \frac{1+j}{\Delta},$$

where Δ is the current penetration depth $\Delta = \sqrt{\frac{2}{\sigma\omega\mu\mu_0}} = \frac{503}{\sqrt{\sigma f\mu}}$.

The solution for H_z is sought in the form:

$$H_z(x) = A\,e^{-kx} + B\,e^{kx} \quad (7)$$

For physical considerations it can be stated that $H_z \neq \infty$, but if $x = \infty$ is substituted in equation (7), we obtain $e^{kx} = \infty$. It directly follows that constant B=0. Therefore, the general solution of (7) is written as follows

$$H_z(x) = H_{zo}\,e^{-kx}, \quad (8)$$

where H_{zo} is the surface field of the metal being heated.

2.2. Definition of boundary condition

To define the surface field of the metal being heated, the following condition is used [7], [8]

$$H_z(0) = H_{z0}. \quad (9)$$

The square contour L (Fig. 1b.) with a cross-section S and a length of its large side l is considered. This contour is intersected by the inductor turns yet not reaching the piece.

After integrating Maxwell equation and applying Stoke's theorem, the following is obtained:

$$H_z(0) = \frac{I\,n}{l}. \quad (10)$$

where: l – the length of the large side of the contour L; n – the number of turns in the square S; I – the complex current amplitude in the turn; $H_z(0)$ - the surface field of the metal being heated.

After substituting equation (9) in (10), the constant H_{z0} is determined and we obtain the solution of the problem (5)-(10)

$$H_z(x) = H_{z0}\,e^{-kx} = \frac{I\,n}{l}\,e^{-kx} \quad (11)$$

2.3. Definition of heat source density

After substituting H_z in (5), the following is obtained for E_y:

$$E_y(x) = -\frac{1}{\sigma + j\varepsilon\varepsilon_0\omega}\frac{dH_z}{dx} = \frac{H_{z0}\,k\,e^{-kx}}{\sigma + j\varepsilon\varepsilon_0\omega} \approx$$
$$\approx -\frac{I\,n}{l}\frac{k\,e^{-kx}}{\sigma}, \quad (12)$$

where σ is piece conductivity.

Heat source density is calculated by using the equation [7], [8]

$$F(x) = \frac{1}{2}JE_y^* = \frac{1}{2}\sigma|E_y|^2 = H_{z0}^2\frac{e^{-2\frac{x}{\Delta}}}{\sigma\,\Delta^2}. \quad (13)$$

participating in the heat conduction equation.

2.4. Additional simplification of heat source density formula

Similar simplification has been used in [8]. By using (14), for the total power transferred in direction x from the surface to the centre, the following is obtained:

$$F_0 = \frac{I^2\,n^2}{l^2}\frac{1}{\sigma\Delta^2}\int_0^\infty e^{-2\frac{x}{\delta}}dx = \frac{I^2\,n^2}{l^2}\sqrt{\frac{f\mu}{\sigma}}\,0{,}993\,10^{-3}. \quad (14)$$

We will consider heating of a cylindrical body of radius R, i.e. $x \in [0, R]$. Let's assume that the entire power is uniformly transferred into a surface layer of thickness ξ, where from $\xi \approx 0.87\,\Delta$. This layer is referred to as the effective depth of current penetration. In this case the heat source density is defined as follows:

$$F(x) = F_0\frac{2\pi R}{\pi\left(R^2 - (R-\xi)^2\right)}h(x) =$$
$$= \frac{F_0}{\xi}\frac{2R}{2R-\xi}h(x) = \frac{F_0}{\xi\left(1-\xi/(2R)\right)}h(x), \quad (15)$$

where $F_0 = \frac{I^2 n^2}{l^2}\sqrt{\frac{f\mu}{\sigma}}\ 0{,}993\ 10^{-3}$;

$h(x) = \begin{cases} 0 & , за\ x \in [0, R-\xi] \\ 1 & , за\ x \in [R-\xi, R] \end{cases}$ and $\xi \approx 0{,}87\Delta$.

2.5. Thermal problem

The processes related to heat transfer in rigid bodies are non-stationary since they also depend on time. Solving problems in the area of non-stationary heat conduction means finding the dependence of the temperature field on time where the geometry and body physical properties are set in advance[9], [10], [11].

To solve the thermal problem, we need to solve the heat conduction equation (16) in polar coordinates where the boundary conditions (17) and the initial condition (18) [10] are set in advance:

$$C\rho\frac{\partial U}{\partial t} = \frac{\lambda}{r}\frac{\partial}{\partial r}\left(r\frac{\partial U}{\partial r}\right) + \frac{F_0}{\xi\left(1-\xi/(2R)\right)}h(r), \quad \text{for } r \in [0, R] \text{ and } t \geq 0. \tag{16}$$

$$\lambda\frac{\partial U}{\partial r}(0,t) = 0;\ \lambda\frac{\partial U}{\partial r}(R,t) = 0. \tag{17}$$

$$U(r,0) = 0. \tag{18}$$

where: $U = T - T_\infty$ - temperature of the body being heated, where 273,15 °K is the ambient temperature; ρ – density of the body being heated; C – thermal capacity; λ – thermal-conductivity coefficient; $F(r) = \frac{F_0}{\xi\left(1-\xi/(2R)\right)}h(r)$ - change of the heat source density in the direction of the radius; it is calculated according to the formula (15).

Functions F(r) from (16) are partially smooth functions only with regard to r, but not with regard to t. Therefore, it has an expansion in Bessel function of the form:

$$F(r) = \sum_{k=1}^{\infty} A_k J_0(\nu_k r). \tag{19}$$

where J_0 is Bessel function of first kind of zero order and $\{\nu_k\}$ are the roots of the equation

$$J_1(\nu R) = 0 \tag{20}$$

The solution could be found in the form

$$U(t,r) = \sum_{k=0}^{\infty} T_k(t) J_0(\nu_k r). \tag{21}$$

After substituting (21) in (17), we obtain:

$$-\sum_{k=0}^{\infty}\nu_k T_k(t) J_1(0) = 0$$

$$-\sum_{k=0}^{\infty}\nu_k T_k(t) J_1(\nu_k R) = 0.$$

Since ν_k are the roots of the equation (20) and $J_0'(x) = -J_1(x)$, the result is that (19) is satisfied.

After substituting (21) in (16), we obtain:

$$\sum_{k=0}^{\infty}\rho C T_k'(t) J_0(\nu_k r) - \lambda T_k(t)\{\frac{d^2}{dr^2}J_0(\nu_k r) + \frac{1}{r}\frac{d}{dr}J_0(\nu_k r)\} - A_k J_0(\nu_k r) = 0.$$

However, $J_0(\nu r)$ is a solution of Bessel equation $\frac{d^2y}{dr^2} + \frac{1}{r}\frac{dy}{dr} + \nu^2 y = 0$. Thus the kind obtains the following form

$$\sum_{k=0}^{\infty}\{\rho C T_k'(t) + \lambda\nu_k^2 T_k(t) - A_k\} J_0(\nu_k r) = 0.$$

The last equations are satisfied if

$$\rho C T_k'(t) + \lambda\mu_k^2 T_k(t) - A_k = 0 \text{ for } k = 0,1,2,\ldots. \tag{22}$$

After substituting (21) in (18), we obtain:

$$\sum_{k=0}^{\infty} T_k(0) J_0(\nu_k r) = 0.$$

That is satisfied when

$$T_k(0) = 0 \text{ , for } k = 0,1,2,\ldots. \tag{23}$$

From (22) and (23) the following system is obtained:

$$\begin{cases} \rho C T_k'(t) + \lambda\nu_k^2 T_k(t) - A_k = 0 \\ T_k(0) = 0 \end{cases}, \text{ for } k = 0,1,2,\ldots.$$

The solution of this system is as follows:

$$T_0(t) = \frac{A_0}{\rho C}t, \text{ since } \nu_0 = 0$$

$$T_k(t) = \frac{A_k}{\lambda\nu_k^2}(1 - e^{-\frac{\lambda\nu_k^2}{\rho C}t}) \text{ , when } k = 1,2,\ldots$$

The expression for is substituted in (21) and the following is obtained:

$$U(t,r)=\frac{A_0}{\rho C}t+\sum_{k=1}^{\infty}\frac{A_k}{\lambda\nu_k^2}(1-e^{-\frac{\lambda\nu_k^2}{\rho C}t})J_0(\nu_k r) \quad (24)$$

The next step is to find coefficients A_k in the expansion of $F(x)=\frac{F_0}{\xi(1-\xi/(2R))}h(r)$, where $h(r)=\begin{cases}0 & , for\ x\in[0,R-\xi]\\ 1 & , for\ x\in[R-\xi,R]\end{cases}$ in Bessel functions $\{J_0(\nu_k r)\}$.

Similar to [4], it can be shown that with regard to the scalar product

$$\int_0^R r J_0(\nu_i r)J_0(\nu_j r)dr = \begin{cases}0, & for\ i\neq j\\ \frac{R^2(J_1^2(\nu_i R)+J_0^2(\nu_i R))}{2}, & for\ i=j\end{cases} \quad (25)$$

those functions are orthogonal.

Using the representation (19) and the scalar product (25) for coefficients, the following is obtained.

$$A_0=\frac{2}{R^2}\int_0^R rF(r)J_0(0)dr=$$

$$=\frac{2F_0}{R^2\xi(1-\xi/(2R))}\int_{R-\xi}^R rdr=\frac{(2R-\xi)F_0}{R^2(1-\xi/(2R))}$$

$$A_k=\frac{2}{R^2(J_1^2(\nu_k R)+J_0^2(\nu_k R))}\int_0^R r\,F(r)J_0(\nu_k r)dr=$$

$$=2\frac{R\,J_1(\nu_k R)-(R-\xi)\,J_1(\nu_k(R-\xi))}{\nu_k\,R^2(J_1^2(\nu_k R)+J_0^2(\nu_k R))}\frac{F_0}{\xi(1-\xi/(2R))}.$$

When integrating, we use $\frac{d}{dx}\left(x^n J_n(x)\right)=x^n J_{n-1}(x)$.

After substituting coefficients A_k in (25), we obtain

$$U(t,r)=\frac{(2R-\xi)F_0}{R^2(1-\xi/(2R))\rho C}t+$$
$$+\sum_{k=1}^{\infty}2F_0\frac{R\,J_1(\nu_k R)-(R-\xi)\,J_1(\nu_k(R-\xi))}{\xi(1-\xi/(2R))R^2(J_1^2(\nu_k R)+J_0^2(\nu_k R))\,\lambda\,\nu_k^3}. \quad (26)$$
$$.(1-e^{-\frac{\lambda\nu_k^2}{\rho C}t})J_0(\nu_k r)$$

where $\{\nu_k\}$ are the roots of the equation $J_1(\nu R)=0$,

$$F_0=\frac{I^2\,n^2}{l^2}\frac{1}{2\sigma\delta}=\frac{I^2\,n^2}{l^2}\sqrt{\frac{f\mu}{\sigma}}\ 0{,}993\ 10^{-3},$$

$$\Delta=\sqrt{\frac{2}{\sigma\omega\mu\mu_0}}=\frac{503}{\sqrt{\sigma f\mu}}\ \text{ and }\ \xi\approx 0.87\,\Delta.$$

3. Implementation of the mathematical model

With volumetric heating inductors, pieces of total mass of several tens to 100-150 kg are heated in the inductor. Those pieces move inside the inductor at a specific delivery cycle so that the temperature around the boundary can be up to 1300 °C and the difference between the hottest and coldest part of the piece can be less than 150 °C. That temperature field is suitable for further machining of the piece by applying forging and pressing.

To test the proposed mathematical model, the technical characteristics of a volumetric heating machine R–ITO–630/1–A–L with a SMK UB 2F2 power source are used.

The volumetric heating machine of R–ITO–630/1–A–L type has a cylindrical inductor, a capacitor cabinet and an automated device for single delivery of the pieces to the inductor. The heated pieces on the conveyor belt are delivered to the heat treatment machines. A set of R–ITO inductors is used for pieces of diameter 60-130 mm, and shown in Fig. 2.

Figure 3. presents the voltage and current through a thyristor inverter at a piece diameter of Ø 110 and a delivery cycle of 60 s. The oscillogram indicates a 403 A current through the thyristor inverter. Since two current-driven inverters operate in parallel in the transducer, the total current is 806 A. The voltage is 620 V.

Figure 4. shows the voltage and current of the inductor at a piece diameter of Ø 110 and a delivery cycle of 60 s.

Figure 2.General view of a volumetric heating machine of R–ITO–630/1–A– L type

The inductor is calculated upon the following output parameters: power source frequency f = 900 Hz; inductor supply voltage U = 600 V; piece diameter D_2 = 110 mm; piece length a_2 = 150 mm; output temperature T = 1250 ÷ 1300 °C; maximum

temperature difference between the surface and piece center ΔT = 150 °C. The very calculation is done according to the methodology described in [1], [2] for cylindrical pieces of diameter ø 110 for an R – ITO 100 – 130 D inductor. Calculation results are presented in Table 1.

Table 1. Calculated equivalent parameters of R – ITO 100 – 130 D inductor at a piece ø 110.

Piece diameter, mm / mass, kg	110/11,19
r_i, Ω	8,39.10-3
X_i, Ω	4,77.10-2
Z_i,Ω	4,84.10-2
I_i, A	4034
$I_{power\ source}$, A	806
$P_{power\ source}$, kW	159
cos φ	0,173
Inductor diameter, D_1, mm	180
Inductor length,a_1, mm	3000
Number of inductor turns	39

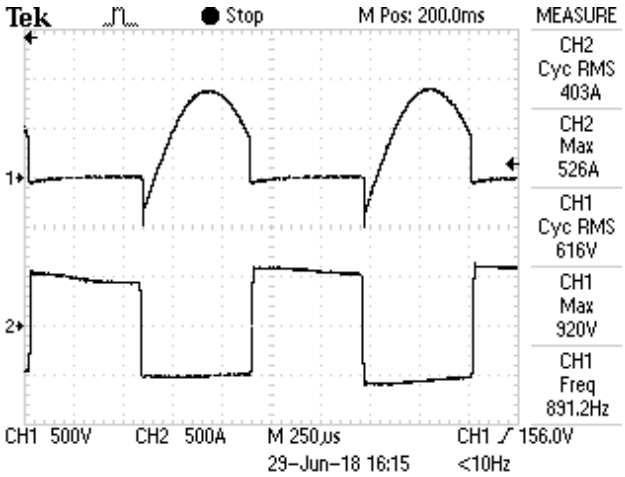

Figure 3. Current and voltage of a thyristor inverter at a piece diameter Ø 110

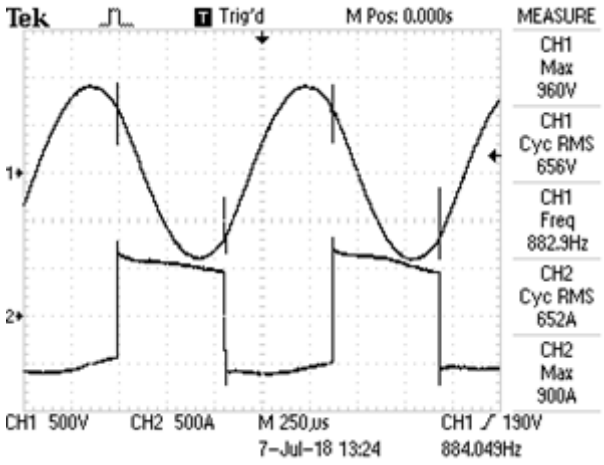

Figure 4. Current and voltage of the inductor at a piece diameter Ø 110

On the basis of the proposed mathematical model, the temperature of the pieces is modeled in MATLAB at set electrical mode of the volumetric heating machine.

We would like to remind that the temperature analysis of the inductor thermal mode is done taking into account the following simplifications: the volumetric heating inductor is considered as a system thermally insulated from the ambient space and the temperature of each single piece is assumed to be equal across its cross-section. In addition, parameters C, λ, σ and μ, which characterize the conducting medium, considerably depend on the temperature and magnetic field [12], [13], [14]. A significant change of μ occurs before and after the Curie point.

In order to eliminate that problem, the following simplification is done. A model where heating is modeled in two phases is considered. The first phase is heating below the Curie point and averaged parameters which are appropriate for that temperature range are used. The second one is heating above the Curie point (assumed to be 780 °C) and other averaged parameters are used. The transition from the first values to the next ones is incremental thus leading to a sharp change of the simulated temperature field around the Curie point. Of course, such an effect cannot be observed if parameters are gradually changed. The further proposed verification by means of Comsol Multiphysics shows that this ununiformity is only of local nature, i.e. it is observed only around the Curie point [15].

The temperature processes are modeled in several variants defined by a set piece diameter, different delivery cycles and other identical conditions. The results are illustrated in Fig. 5. – Fig. 8.

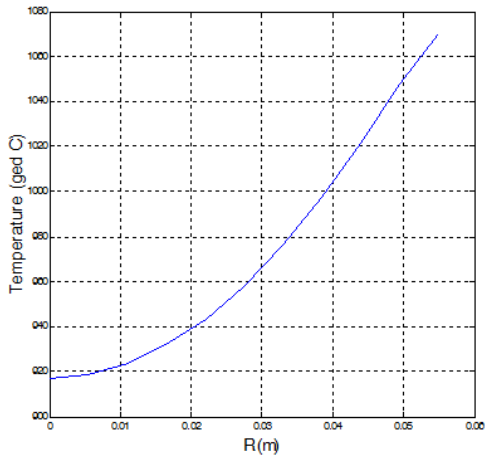

Figure 5. Temperature distribution across the cross section of the piece being heated at a delivery cycle of 60 s.

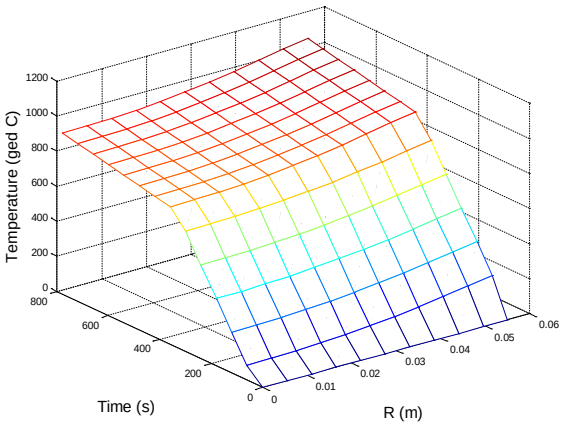

Figure 5a. Dependence of temperature on the cross-section of the piece being heated and heating time at a delivery cycle of 60 s.

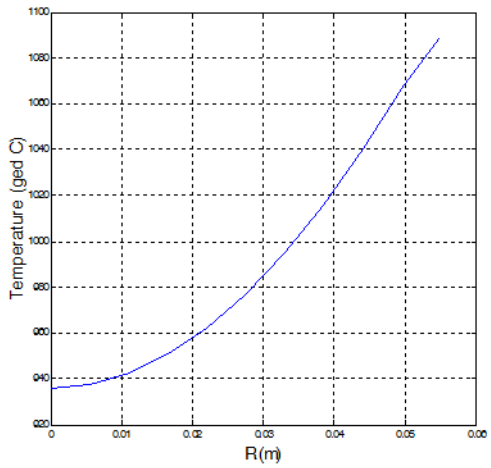

Figure 6. Temperature distribution across the cross section of the piece being heated at a delivery cycle of 65 s.

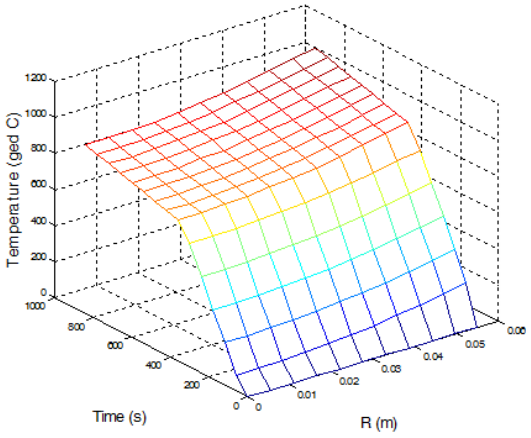

Figure 6a. Dependence of temperature on the cross-section of the piece being heated and heating time at a delivery cycle of 65 s.

The above figures present the results from the temperature distribution across the cross-section of the metal being heated from the centre to the surface. The maximum difference does not exceeed 170 °C, which is admissible for the subsequent technological operations. Heating of a piece at a delivery cycle of 60 s. and 65 s. is simulated, which means respectively a 13- and 14-minute stay in the inductor. The results indicate that at a delivery cycle of 60 s. the output temperature of pieces is low for the technological operations where as at a delivery cycle of 65 s. is high. It could be assumed that at a delivery cycle of 60 s. the piece temperature is close to the optimal one for the subsequent forging and pressing operation.

To verify the results obtained from the mathematical model, Comsol Multiphysics application is used. It operates using the finite element method [15], [16]. Within this model the parameters change gradually in the course of heating [17], [18], [19].

The dependences of the piece specific conductivity σ and magnetic permeability μ on the temperature for medium-carbon steels published in works [4] are presented by the expressions:

$$\mu = -1{,}69.10^{-14}.T^{5{,}334} + 39{,}57 \text{ for the interval}$$

$$20°C \leq T \leq Tc, \quad (27)$$

$$\mu = 1 \text{ for the interval } T \geq Tc, \quad (28)$$

where T – piece temperature, Tc – Curie temperature which varies with different steel brands, for pure iron it is about 780 °C.

The specific conductivity σ is defined by the expression:

$$\sigma = \left(14{,}88.T^{-0.2036} - 2{,}717\right)10^{6} \quad (29)$$

where T – piece temperature.

Figure 7. illustrates the implemented model after a stay of different duration of the pieces in the inductor, i.e. at a different delivery cycle. Parameters and data from running volumetric heating machines are used as input data for modelling the thermal mode in the inductor and forming temperature zones along the length. The required input data are summarized in Table 2.

Table 2. Required parameters

Symbol	Parameter	Value
D_1 ,mm	Inductor diameter	ø180
D_2 ,mm	Piece diameter	ø110
a_1,mm	Inductor length	3000
a_2,mm	Piece length	300
n	Number of inductor turns	39
T, s	Delivery cycle of pieces	50 55 60 65
I, A	Inductor current	4000

Table 3. presents the required physical parameters and constants of medium-carbon steel.

Table 3. Physical parameters of the piece being heated

Temperature, ° C	0	350	500
Heat conduction λ, W/(m·° C)	52	43	35
Specific thermal capacity J/(kg·K)	540	600	650
Density, kg/m^3	7850	7731	7700
Magnetic permeability, μ	40	38	37
Conductivity σ, GS/m	5	2	1.4
Temperature, ° C	750	1000	1250
Heat conduction λ, W/(m·° C)	30	28	30
Specific thermal capacity J/(kg·K)	750	1300	1500
Density, kg/m^3	7660	7483	7380
Magnetic permeability, μ	24	1	1
Conductivity σ, GS/m	1,10	0,9	0,83

Figure 8. presents the results for the temperature field at the inductor output obtained in Comsol Multiphysics at a different delivery cycle of 50, 55, 60 and 65 s.

The results shown in Fig. 8 illustrate the temperature distribution across the piece cross-section at the inductor output. They confirm the accuracy of the proposed mathematical model. The temperature on the piece surface at a delivery cycle of 60 s. is 1220 °C and the one obtained from the mathematical model is 1208 °C. The temperature in the piece centre shown in Fig. 8. is 1109 °C and the one in Fig. 6. is 1040 °C. When those results are compared, it is found that the difference does not exceed 6 %.

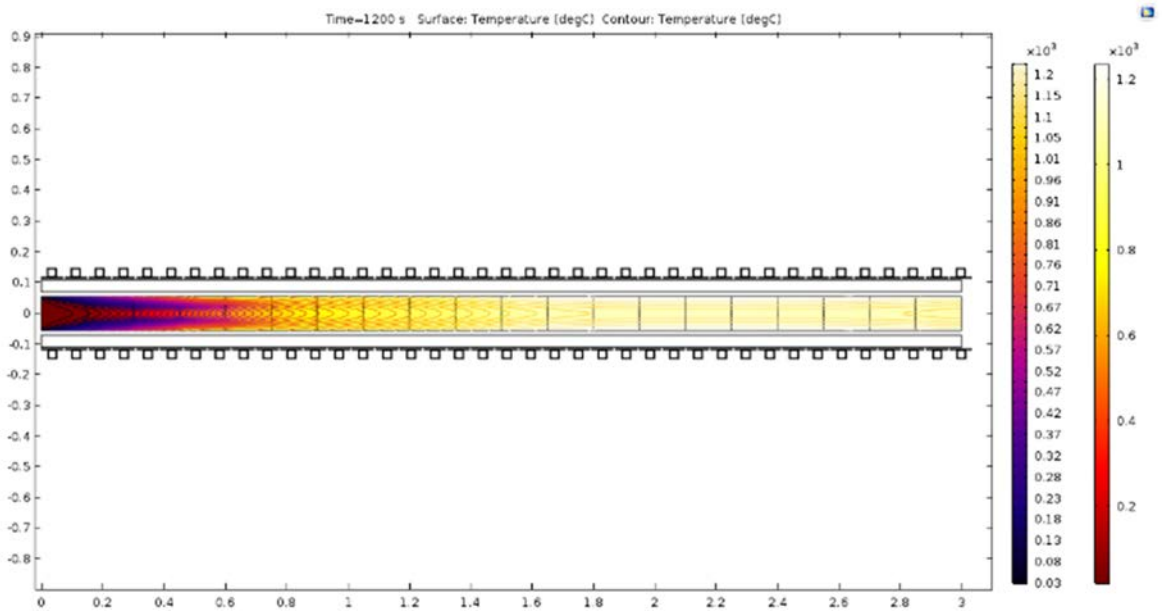

Figure 7. Temperature distribution across the cross-section of the piece being heated at a delivery cycle of 60 s.

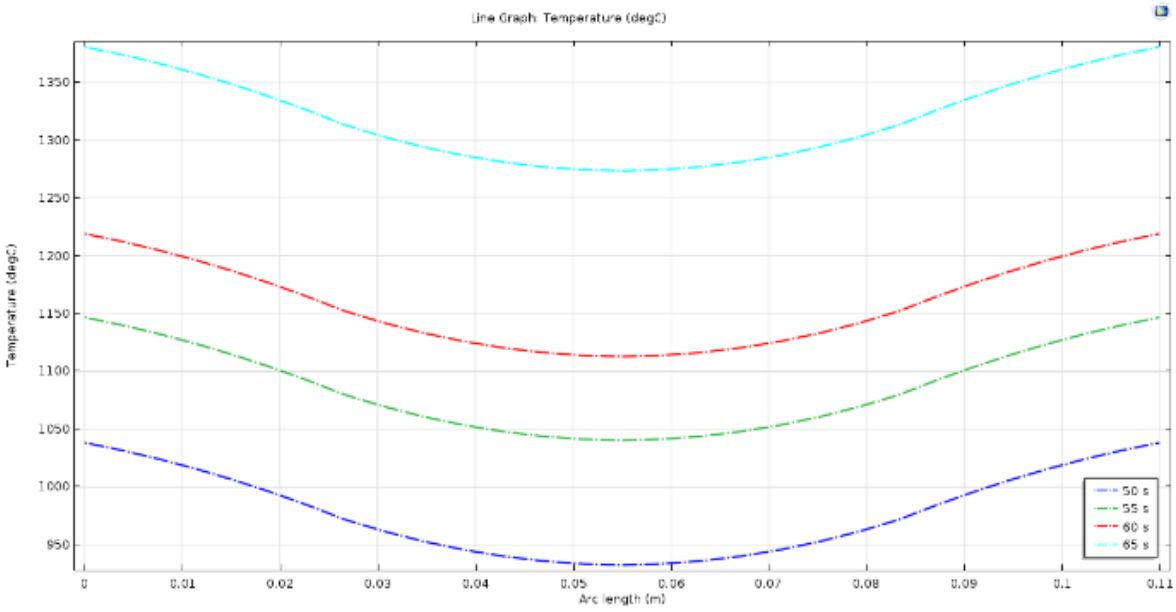

Figure 8. Temperature distribution across the cross-section of the piece being heated at a delivery cycle of 50, 55, 60 and 65 s.

4. Conclusion

The present publication presents the results from a mathematical model of the volumetric induction heating process. The results have been compared to the implemented modeling of the electromagnetic and temperature field in Comsol Multiphysics. The obtained results demonstrate the adequacy of the proposed model. The error does not exceed 6 %. It is caused by the different way of reading the change in the medium parameters in the course of heating. The subject of our future work will be the improvement of the model for indicating the convective heat transfer and the radiation of the heated pieces, as well as for applying it to a heating process control system.

Acknowledgements

The carried out research is realized in the frames of the project "Model based design of power electronic devices with guaranteed parameters", ДН07/06/15.12.2016, Bulgarian National Scientific Fund.

References

[1]. A.E. Slukhotskii, S.E. Ryskin (1974). Inductors for Induction Heating, Energy Publications, St. Petersburg, Russia.
[2]. A.E. Slukhotskii, V.N. Nemkov, N.A. Pavlov, A.V. Bamuner (1981). Induction Heating Equipment, Energoizdat Publishers, St.Petersburg.
[3]. Rudnev, V., Loveless, D., & Cook, R. L. (2017). *Handbook of induction heating*. CRC press.
[4]. V. Rudnev, G. Totten (editors) (2014). ASM Handbook Volume 4C: Induction Heating and Heat Treating, ASM International, Materials Park, OH.
[5]. V. Rudnev, D. Loveless (2014). Induction hardening: Technology, process design, and computer modeling, in Comprehensive Materials Processing, G. Krauss (editor), Elsevier Ltd., Oxford, UK, Vol. 12.
[6]. V. Rudnev, R. Cook, D. Loveless, M. Black (2007). Induction heat treatment; Basic principles, computation, coil construction, and design considerations, Chapter 4, in Steel Heat Treatment: Equipment and Process Design, G.E. Totten (editor), CRC Publishing, New York.
[7]. J.D. Jackson (1998). Classical Electrodynamics, 3rd edition, Jon Wiley&Sons.
[8]. D. A. Lowther, P. P. Silvester (1986). Computer-Aided Design in Magnetics, Springer-Verlag, Berlin.
[9]. Carslaw H.S., J.C. Jager (1946). Condition of Heat in Solids, Clarendon Press, Oxford.
[10]. Feliachi, M., & Develey, G. (1991). Magneto-thermal behavior finite element analysis for ferromagnetic materials in induction heating devices. *IEEE transactions on magnetics*, *27*(6), 5235-5237.
[11]. Skoczkowski, T. P., & Kalus, M. F. (1989). The mathematical model of induction heating of ferromagnetic pipes. *IEEE Transactions on Magnetics*, *25*(3), 2745-2750.
[12]. K. Schroder (1983), CRC Handbook of Electrical Resistivities of Binary Metallic Alloys, CRC Press, Inc., Boca Raton,FL.
[13]. Lupi, S., & Rudnev, V. (2014). Electromagnetic and thermal properties of materials. *ASM Handbook Volume 4C: Induction Heating and Heat Treatment*, 28-35.
[14]. T.L. Bergman, D.P. Dewit, A.S. Lavine, F.P. Incropera (2011). Fundamentals of Heat and Mass Transfer, John Wiley & Sons, NJ.
[15]. Bay, F., Labbé, V., Favennec, Y., & Chenot, J. L. (2003). A numerical model for induction heating processes coupling electromagnetism and thermomechanics. *International journal for numerical methods in engineering*, *58*(6), 839-867.

[16]. Bullo, M., D'Ambrosio, V., Dughiero, F., & Guarnieri, M. (2007). A 3-D cell method formulation for coupled electric and thermal problems. *IEEE Transactions on Magnetics*, *43*(4), 1197-1200.

[17]. Canova, A., Dughiero, F., Fasolo, F., Forzan, M., Freschi, F., Giaccone, L., & Repetto, M. (2009). Identification of equivalent material properties for 3-D numerical modeling of induction heating of ferromagnetic workpieces. *IEEE Transactions on Magnetics*, *45*(3), 1851-1854.

[18]. Monzel, C., & Henneberger, G. (2002). Temperature solver for highly nonlinear ferromagnetic materials for thin moving sheets in transversal flux induction heating. *IEEE transactions on magnetics*, *38*(2), 937-940.

[19]. Acero, J., Alonso, R., Barragán, L. A., & Burdio, J. M. (2006). Modeling of planar spiral inductors between two multilayer media for induction heating applications. *IEEE transactions on magnetics*, *42*(11), 3719-3729.